Available online at www.sciencedirect.com
ScienceDirect
Ceramics International 36 (2010) 879–885
CERAMICS INTERNATIONAL
www.elsevier.com/locate/ceramint

Effect of alumina addition on initial sintering of cubic ZrO_2 (8YSZ)

Gustavo Suárez, Yoshio Sakka *

Nano Ceramic Center, National Institute for Materials Science, 1-2-1, Sengen, Tsukuba-shi, Ibaraki 305-0047, Japan

Received 20 October 2008; received in revised form 9 April 2009; accepted 3 October 2009
Available online 13 November 2009

Abstract

The effect of 0–10 wt% alumina addition on the initial sintering of 8 mol% Y_2O_3 cubic ZrO_2 (8YSZ) was studied. Activation energy and initial stage of sintering mechanism were analyzed in order to understand the effect of the alumina in the sintering process. The analysis was carried out using the analytical method for constant rate heating (CRH). The activation energy decreased from 716 to 599 kJ/mol for undoped 8YSZ to 2.16 wt% of alumina–8YSZ, respectively. The mechanism for the initial stage of sintering for <2.16% Alumina–8YSZ changed from grain boundary diffusion (GBD) to volumetric diffusion (VD). With 10 wt% of alumina, the activation energy increased to 854 kJ/mol which was thought due to the change in the initial stage of sintering mechanism from VD to GBD.

Keywords: Cubic zirconia; Sintering mechanism; Alumina addition

1. Introduction

The addition of 8 mol% Y_2O_3 stabilizes the cubic fluorite structure of ZrO_2, from room temperature to its melting point. 8YSZ is the most common electrolyte in oxide fuel cells because the material possesses excellent oxygen ion conductivity and exhibits desirable stability in both oxidizing and reducing atmospheres [1,2]. The excellent ionic conductivity of this material can be achieved through the development of fine and homogeneous microstructures. In order to obtain these microstructural properties, it is necessary to control the powder characteristics, the forming process and especially the sintering conditions.

The addition of Al_2O_3 to zirconia ceramics has been previously studied for its effect on different property aspects, e.g. grain growth [3,4], superplasticity [5], phase transformation and phase composition [6–8]. Previous studies have also reported on the activation energy for the sintering process for the system ZrO_2–Al_2O_3 [9–11].

The initial stage of sintering for various ceramics has been studied by a number of researchers and many equations were developed to analyze the quantitative kinetics. The first reports on aspects of sintering kinetics were presented by Kingery and Berg [12], followed by other researchers [13–17] who developed equations for both, isothermal and non-isothermal sintering conditions. Recently Matsui et al. [9] also developed an analytical method that can be used to determine the diffusion mechanism at the initial sintering stage by employing a constant rate of heating (CRH) technique. The current authors [9] propose a useful combination of the equation developed by Young–Cutler [17] and Wang–Raj [11].

In the present study, the authors analyze the effect on the initial sintering stage of 8YSZ with small and large additions of alumina using the combination of equations developed by Matsui et al. [9]. The effects on the activation energy and the sintering mechanism for initial stage were studied for all the additions. We also propose an explanation for the change in the observed sintering mechanism from grain boundary diffusion (GBD) without the alumina additive to volumetric diffusion (VD) for small amounts of alumina and the increment in activation energy and the change back to the GBD mechanism for the addition of 10%wt of Al_2O_3.

2. Experimental procedure

2.1. Samples preparation

The starting materials were 8YSZ powder containing 7.8 mol% of Y_2O_3 (TZ-8Y, SiO_2 content 0.003 wt% grade, Tosoh, Japan) and high-purity Al_2O_3 powder (>99.99%, SiO_2

* Corresponding author. Tel.: +81 29 859 2461; fax: +81 29 859 2401.
E-mail address: SAKKA.Yoshio@nims.go.jp (Y. Sakka).

0272-8842/$36.00
doi:10.1016/j.ceramint.2009.11.003

content 3 ppm TM-DAR, Taimei Chemicals, Nagano, Japan) with a particle size averaging 0.15 μm. The samples were prepared adding 0.65, 2.16 and 10 wt% of alumina to 8YSZ powder. The powders were dispersed in water with the appropriate amount of a polyelectrolyte (poly(ammonium carboxylate), ALON A-6114, Toagosei Co., Tokyo, Japan) dispersed in distilled water [18]. Aqueous suspensions were prepared containing 30 vol% solids content of the ZrO_2 and Al_2O_3 powder mixtures. Long-range segregation caused by the difference in particle size and/or density has been confirmed to be inhibited by hindering sedimentation if the solid content exceeds 30 vol% in suspensions [19].

The suspension of the ZrO_2 and Al_2O_3 powder mixture is stabilized by electrosteric repulsion [20]. The suspension was dispersed ultrasonically for 10 min and stirred using a magnetic stirrer at room temperature. The ultrasonic irradiation (Model USP-600, Shimadzu, Tokyo, Japan) was conducted at 20 kHz. Suspensions were evacuated in a desiccator to eliminate air bubbles after which they were slip cast into plaster molds with a 0.2 μm porous Teflon film separating the slurry from the mold forming 4 cm × 4 cm × 0.5 cm consolidated compacts. Cold isostatic pressing (CIP) at 400 MPa was conducted to improve green density.

The homogeneous compacts were heated and their shrinkage was measured using a thermomechanical analyzer (TMA; System TMA8310, Rigaku, Tokyo). The measurements with CRH were performed in the range from room temperature to 1400 °C at heating rates of 2.5, 5, 10 and 20 °C/min with no holding time. SEM pictures were taken from samples sintered at 1300 °C for 2 h. Densities of the green and sintered bodies were measured by the Archimedes method using kerosene or water.

2.2. Analysis of sintering shrinkage

The sintering–shrinkage experimental data was obtained using TMA. Assuming isotropic shrinkage to green compact, the density $\rho(T)$ at given temperature T is given by the following equation (Eq. (1)) [11].

$$\rho(T) = \left(\frac{L_f}{L(T)}\right)^3 \rho_f \tag{1}$$

Where $\rho(f)$ is the final density, L_f and $L(T)$ are the final length and the length at temperature T of the specimen.

As previously mention we used the method described by Matsui et al. [9,21–23], where they have incorporated a combination of equations developed by Young–Cutler [17] and Wang–Raj [11] both based on the two-spheres shrinkage model.

Raj et al. derived the sintering rate equation as follows:

$$\ln\left[Tc\left(\frac{d\rho}{dT}\right)\right] = -\frac{Q}{RT} + \alpha_{1/n} \tag{2}$$

where $\alpha_{1/n}$ is the frequency factor given by:

$$\alpha_{1/n} = \ln[f_{1/n}(\rho)] + \ln\left[\frac{K\gamma\Omega D_0}{k}\right] - p\ln a \tag{3}$$

T is the absolute temperature, c is the heating rate, Q is the activation energy, R is the universal constants of gases, $f_{1/n}(\rho)$ is a function of density, K is a numerical constant, Ω is the atomic volume, γ is the surface energy, D is the diffusion coefficient, k is the Boltzmann's constant, p is a parameter and a is the spherical particle radius.

Young and Cutler [17] derived the sintering equation for constant heating rate as follows.

$$\frac{d(\Delta L/Lo)}{dT} = \left(\frac{K\gamma\Omega DoR}{ka^p cQ}\right)^n \left(\frac{nQ}{RT^{2-n}}\right)\exp\left(-\frac{nQ}{RT}\right) \tag{4}$$

where a is the particle radius, n and p are parameters depending on the diffusion mechanism and ΔL (=$Lo - L$) is the change in length of specimen. The values of p for GBD and VD are $p = 4$ and $p = 3$, respectively [15]. All these equations, (1)–(4), are applicable for shrinkages <4%, which satisfy the initial or early stage sintering condition studied here.

Using CRH techniques, we can determine the activation energy and the sintering mechanism rearranging and simplifying Eqs. (2) and (4) as follows. From the slope of the Arrhenius-type plot $\ln[Tc(\mathrm{d}\rho/\mathrm{d}T)]$ vs. $1/T$, the activation energy is determined by

$$Q = -RS_1 \tag{5}$$

Using the slope S_2 by re-arrangement of Eq. (4) and graphing $\ln[T^{2-n}(d(\Delta L/Lo)/dT)]$ vs. $1/T$ we can obtain the apparent activation energy expressed as

$$nQ = -RS_2 \tag{6}$$

Since n was in the range $n = 0.31$–0.50 [15], the S_2 parameter can be estimated from the plot of $\ln[T^{1.6}(d(\Delta L/Lo)/dT)]$ against $1/T$. Combining Eqs.(5) and (6) we have

$$n = \frac{nQ}{Q} = \frac{S_2}{S_1} \tag{7}$$

Eqs. (5)–(7) were used to determine the values of activation energy and sintering mechanism in the initial stage of sintering using the results of the CRH experiments.

3. Results and discussion

3.1. Densification and densification rate

Fig. 1A shows the difference in the relative density of the samples with different amount of alumina for the same 5 °C/min CRH. It can be observed the effect of the alumina addition on the densification as follows. Initially for a small addition, the density increases faster than for pure 8YSZ and the three doped samples achieve a good final density. The sample with 10% of alumina had the lowest densification rate and the lowest final density.

The same conclusion can be obtain if we see the densification rate shown in Fig. 1B where we can observe the fastest densification for samples with small amount of alumina. We can also see that the densification process start around 1050 °C. In Fig. 1A, is plotted the densification for

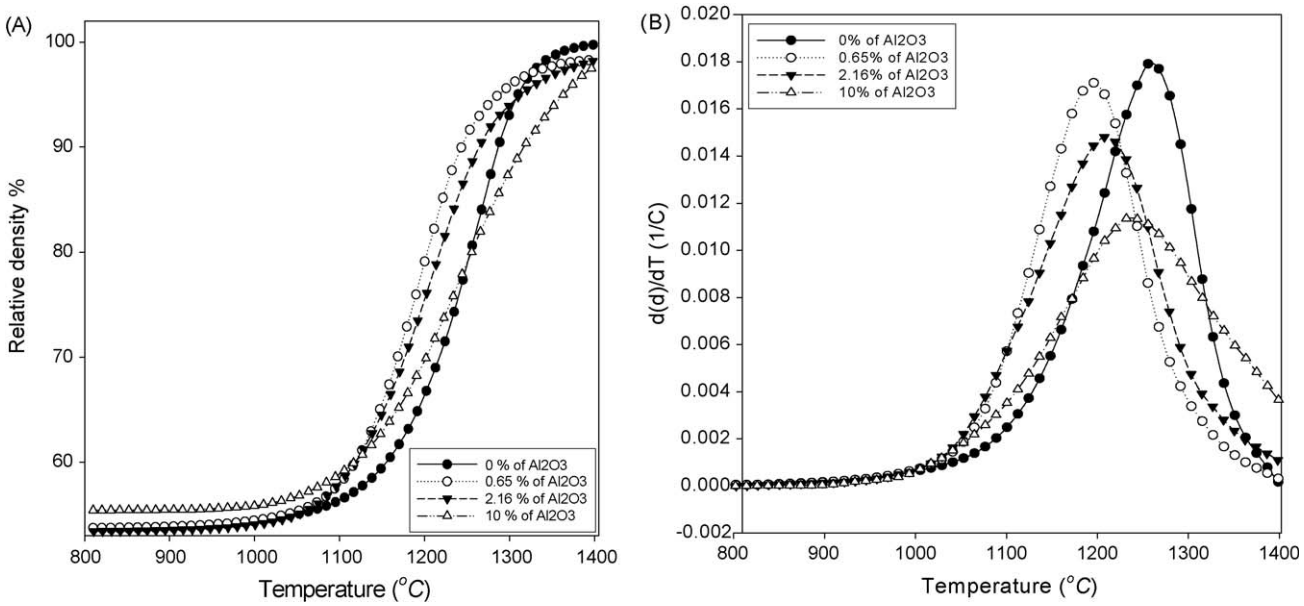

Fig. 1. Temperature dependence of (A) densification and (B) densification rate for CRH run at 5 °C/min with different amounts of Alumina as indicated.

Table 1
Activation energy, sintering mechanism, green and final density for the initial and early stage sintering of CSZ with and without alumina addition. GBD: grain boundary diffusion; VD: volumetric diffusion. The kinetic data is related with the initial stage sintering and the final density is calculated from 2.5 °C/min and 2 h holding time.

Alumina (wt%)	Activation energy (kJ/mol)	n	Sintering mechanism	Rel. Dens. (%)	
				Green	Final
0.00	716	0.31	GBD	54.0	99.0
0.65	624	0.45	VD	53.8	99.5
2.16	599	0.46	VD	53.5	99.2
10.00	854	0.31	GBD	55.4	98.5

samples with different initial green densities (Table 1), for that reason the final density seems to be similar for all compositions. In fact, the addition of small amount of alumina is already shown to be effective for improving the densification [10,21].

In Fig. 2A and B we can observe that the densification rate shifts to higher temperatures when the heating rate is increased and we can also observe that adding a small amount of alumina the sintering process start at lower temperatures independent of the heating rate.

3.2. Activation energy

Fig. 3 shows the graph of Eqs. (2) and (4) where S_1 is the slope of $\ln[Tc(d\rho/dT)]$ vs. $1/T$ and S_2 is the slope of $\ln[T^{2-n}(d(\Delta L/Lo)/dT)]$ vs. $1/T$, both Eqs. (2) and (4) are plotted in the same graph. The activation energy is calculated for each composition from the Arrhenius-type plot, as is given by Eq. (5).

As can be seen from Table 1, the activation energy determined here decreases with the addition of small amounts of alumina (<2.16%). This result is in agreement with those of Matsui et al. [9,22,24] and Wang and Raj [10], and confirms that alumina added in small amounts assists the early stage sintering process. Matsui et al. [9] also suggest that the reason for the decreasing of the activation energy is directly related with the reduction of the surface energy of zirconia powder by inclusion of a small amount of alumina. Aktas and coworkers [4] suggest that this behavior is due to Al^{3+} solute ions segregation in grain boundary region.

It was also suggested by Tekeli and Demir [3] that a small amount of alumina improves densification, while a large amount of alumina decreases the sintering rate. Tekeli et al. proposed that for large amounts the alumina is deposited directly in the grain boundaries and reduces the contact points between zirconia particles. It is known [17,21,23] that the GBD is the predominant initial sintering mechanism for Zr^{4+} and Y^{3+} matter transport in alumina-free samples and this mechanism is affected by the presence of alumina particles. Alumina and zirconia (with no yttria) has very limited mutual solubility and the solubility of Al_2O_3 in ZrO_2 increases as the temperature increase [25,26]. Stough and Hellman [27] reported that alumina can be solved at a temperature of 1200–1600 °C in 0.2–0.3 wt%. These results demonstrate that for additions of alumina more than 0.3 wt% segregation of alumina will exist. This lack of solubility and segregation is due to two main factors. One, strain energy relaxation that results from the size mismatch between the solute and the host ions and, secondly, electrostatic charge compensation [28,29].

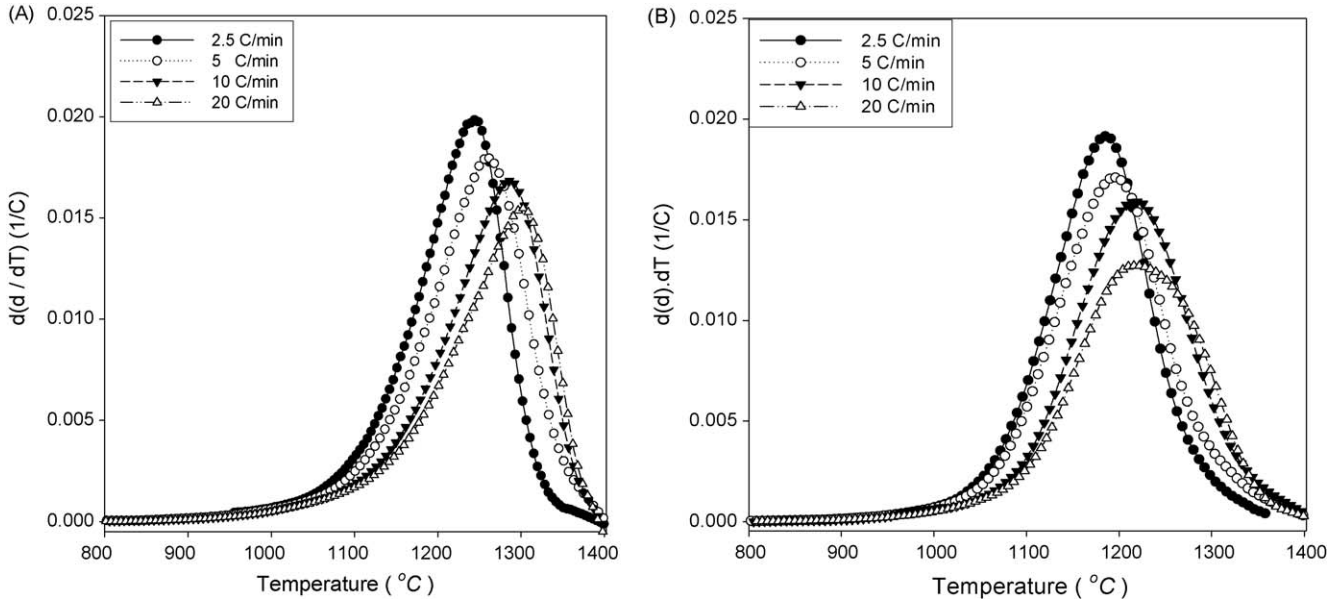

Fig. 2. Densification rates for (A) samples with 0% of alumina and (B) 0.65% of alumina for different CRH.

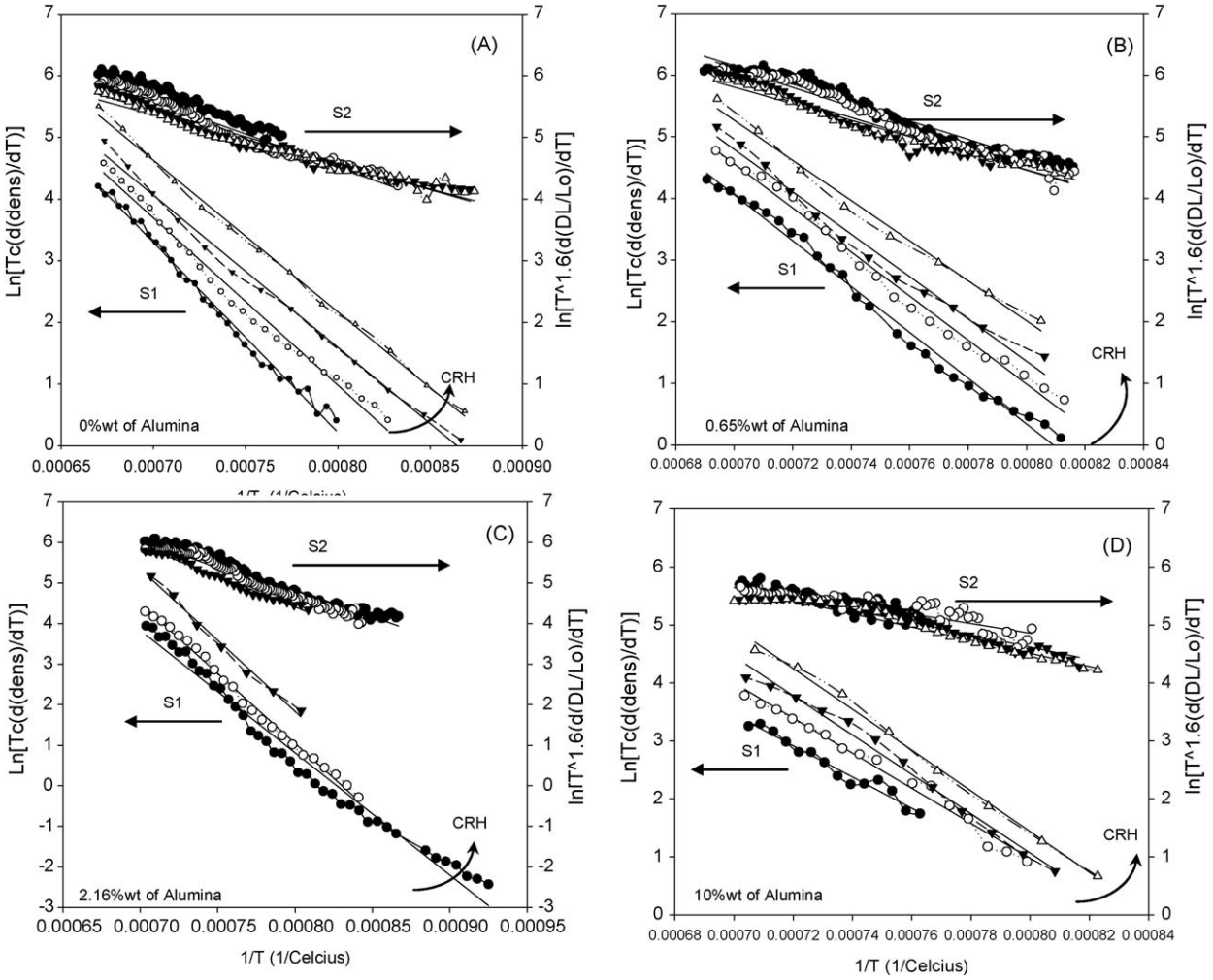

Fig. 3. Plots showing S_1 and S_2 parameters, calculated using the Arrhenius type plot from Eqs. (2) and (4). Each curve is for a different CRH. (A) 0 wt% of Al_2O_3, (B) 0.65 wt% of Al_2O_3, (C) 2.16 wt% of Al_2O_3 and (D) 10 wt% of Al_2O_3.

The variation in the activation energies determined here indicates that the addition of alumina in small amount enhances the initial sintering properties. Other references [4,6–8] also reported that the activation energy for the grain boundary diffusion increases.

For the addition of 10% of alumina the situation is different and we can observe an increase in the activation energy. In previous work by Tekeli and Demir [3], it is suggested that the retardation in the sintering rate and the increment in the activation energy can be attributed to a number of specific reasons. For example, they observed that large amount of alumina (10%) produce porosity in the grain interior and the grain boundaries. This porosity resulted in a diminution on the final sintered density. Another reason is that the distribution of alumina phase in the zirconia matrix induces tensile stress developed by thermal expansion mismatch difference between these two phases. Finally, the diffusion decreases because of the zirconia grains around the alumina particles are unable to contact freely and the path between zirconia grains becomes longer. With this, the diffusion of zirconia becomes slower and this is the reason of the increase in the activation energy when alumina loading is high.

3.3. Sintering mechanism

Using Eq. (7) we estimate the mechanism of the initial stage of sintering from the n values knowing that the values are in the range $n = 0.31–0.33$ for GBD and 0.40–0.50 for VD [15]. Comparing them with the values determined here it is possible to propose a sintering mechanism.

Young and Cutler [17] reported GBD mechanism for pure c-ZrO_2 and Sakka et al. [20,30–34] reported that Zr^{4+} cation diffusion is enhanced at the grain boundaries and that the VD of cations is significantly enhanced by the addition of small amount of alumina. Suárez et al. [35] reported slightly smaller activation energy for undoped 8YSZ using a fast heating rate method (estimated in 400–600 °C/min) concluding that the mechanism is dominated mainly by VD. Due to the characteristic of the experiments Suárez et al. propose that the values for activation energy and diffusion coefficient they calculated by their method are influenced by a combination of mechanisms mainly VD with an important contribution of GBD.

Table 1 shows the results of the activation energy and sintering mechanism determinations. It can be seen that zirconia without alumina sintered via a GBD mechanism as well as small amounts of alumina produce a change in the mechanism from GBD to VD accompanied by a decrease in the activation energy.

The sintering mechanism for 10 wt% of alumina has not been widely reported. We observe that the initial sintering mechanism changes from VD to GBD again and from our results we suggest that can be due to the obstacles that Zr^{4+} cations encounters due to the alumina particles segregated and distributed along the zirconia grain boundaries. As it was reported by Stough and Hellman [27], the solubility of alumina at temperatures in the range of 1200–1600 °C is between 0.2 and 0.3 wt%. In our case, the addition of 0.65 and 2.16% alumina is much higher that the solubility reported by Stough; however once the sintering mechanism changed from GBD in pure 8YSZ to VD for small additions of alumina the initial sintering mechanism remains in VD for the wide range alumina addition between 0.65 and 2.16.

The solubility of alumina in cubic zirconia is not clear and the phase diagrams are not in detailed in this region [27]. Additions of alumina up to 2.16 wt% produce a change in the sintering mechanism from GBD to VD. It is clear that the excess of alumina not soluble must be segregated to the grain boundaries, yet it is not enough to affect the sinterability. Fig. 4 shows the SEM micrograph of the samples sintered at 1300 °C for 2 h of samples with 0, 2.16 and 10 wt% alumina addition. 0.65 wt% is not presented in the picture because no segregation

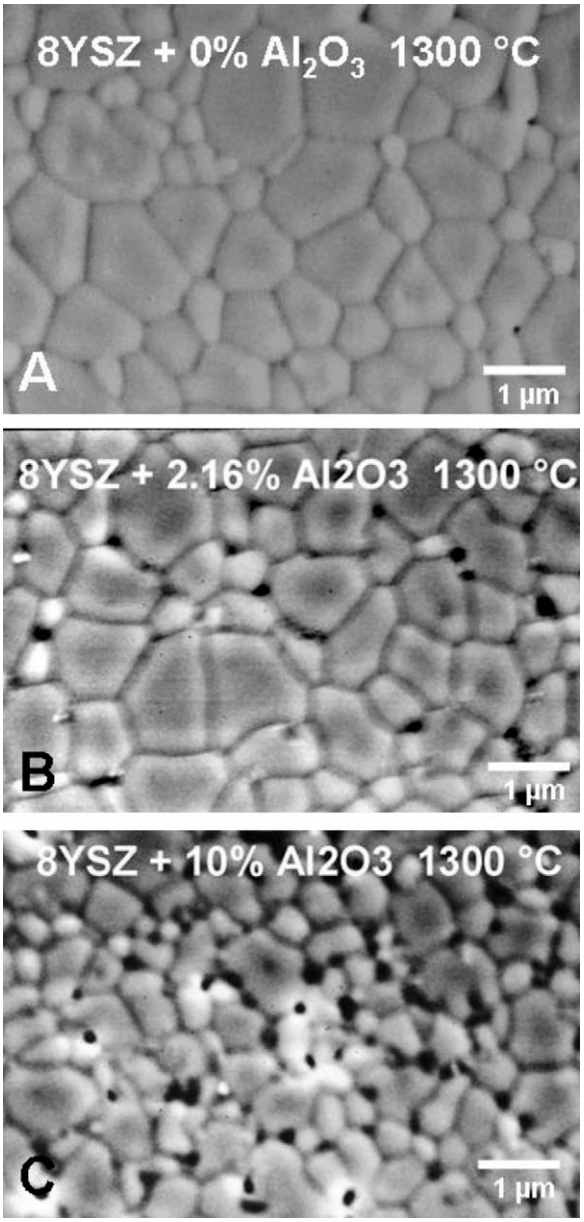

Fig. 4. SEM images of samples with (A) 0 wt%, (B) 2.16 wt% and (C) 10 wt% alumina addition after sintering at 1300 °C for 2 h.

Table 2
Earlier determinations of activation energies and proposed sintering mechanisms for the initial or early stage sintering of CSZ with and without alumina addition. GBD: grain boundary diffusion; VD: volumetric diffusion.

Alumina (wt%)	Activation energy (kJ/mol)	n	Sintering mechanism	Ref.
0	702	0.31	GBD	[9]
0.25	588	0.49	VD	
0	757	0.30	GBD	[22]
0.25	690	0.50	VD	
3.50–96.5	700 ± 100	–	GBD	[10]
0	570	0.25–0.35	VD	[33]

is observed. It can be seen in Fig. 4 that 2.16 wt% already present some alumina segregation but not enough to induce the change in the sintering mechanism. For 10 wt% the segregated alumina is large enough to affect the diffusion of Zr^{4+} cations forcing a change in the mechanism to the GBD mechanism and an increase in the activation energy. This observation is also supported by Sharif and Mecartney [5] presenting SEM micrograph of 8YSZ of 10 wt% alumina with clear segregation to the triple point region.

The results shown in Table 1 are in agreement with the previous experimental results summarized in Table 2. Matsui et al. [9] reported an activation energy for GBD of 702 kJ/mol for undoped cubic zirconia, 588 kJ/mol for 0.23%wt of alumina–8YSZ changing to VD. Matsui et al. [22] also reported 757 kJ/mol in GBD and 690 kJ/mol with VD for cubic zirconia and doped with 0.25 wt% of alumina, respectively. Wang and Raj [10] reported the activation energy to be approximately constant at 700 ± 100 kJ/mol for alumina concentrations between 3.5 and 96.6 wt%, with GBD responsible for the sintering in all ranges of alumina concentration.

4. Conclusion

In this work the authors studied the effect of alumina in the initial or early stage sintering of cubic zirconia using constant rate heating (CRH) techniques and analyzed the results using kinetic equations derived by previous workers. For less than 3 wt% of alumina addition enhances the densification rate and minimizes the activation energy generating a mechanism change from grain boundary diffusion (GBD) to volume diffusion (VD). For a larger amount of alumina (10 wt%) we observed an increase in the activation energy and assumed it was due to the particles of alumina deposited in the grain boundary regions. Our results are in agreement with previously reported data where for small amounts of alumina the reduction in the activation energy is due to the change in the sintering mechanism caused by the migration of Al^{3+} ions segregated to the grain boundaries, so VD dominates. For larger amounts of alumina (10 wt%) the mechanism change again to GBD and the activation energy for initial or early stage sintering increases.

References

[1] N.Q. Minh, Ceramic fuel cells, J. Am. Ceram. Soc. 76 (3) (1993) 563–588.
[2] A.H. Heuer, F.L.W. Hobbs (Eds.), Advances in Ceramics, vol. 3, Science and Technology of Zirconia, American Ceramic Society, Columbus, OH, 1981
[3] S. Tekeli, U. Demir, Colloidal processing, sintering and static grain growth behavior of alumina-doped cubic zirconia, Ceram. Int. 31 (7) (2005) 973–980.
[4] S Tekeli, M. Erdogan, B. Aktas, Influence of alpha-alumina addition on sintering and grain growth behavior of 8 mol% Y_2O_3-stabilized cubic zirconia (c-ZrO_2), Ceram. Int. 30 (8) (2004) 2203–2209.
[5] A. Sharif, M. Mecartney, Superplasticity in cubic yttria stabilized zirconia with 10 wt% alumina, J. Eur. Ceram. Soc. 24 (2004) 2041–2047.
[6] P. Rao, I. Mikio, T. Tanaka, F. Ye, Effect of Al_2O_3 addition on phase composition of ZrO_2 in the Al_2O_3–ZrO_2 system, Ceram. Int. 30 (6) (2004) 923–926.
[7] S. Hong, A. Kakitsui, P. Thompson, Phase transformation in the Al_2O_3–ZrO_2 system, J. Mater. Sci. 33 (1998) 1399–1403.
[8] D. Susnik, J. Holc, M. Hrovat, S. Zupancic, Influence of alumina addition on characteristics of cubic Zirconia, J. Mater. Sci. Lett. 16 (13) (1997) 1118–1120.
[9] K. Matsui, K. Tanaka, N. Enomoto, J. Hojo, Sintering kinetics at constant rates of heating: effect of alumina on the initial sintering stage of yttria-stabilized cubic zirconia powders, J. Ceram. Soc. Jpn. 114 (2006) 763–768.
[10] J. Wang, R. Raj, Activation energy for the sintering of two-phase alumina/zirconia ceramics, J. Am. Ceram. Soc. 74 (8) (1991) 1959–1963.
[11] J. Wang, R. Raj, Estimate of the activation energies for boundary diffusion from rate-controlled sintering of pure alumina, and alumina doped with zirconia or titania, J. Am. Ceram. Soc. 73 (5) (1990) 1172–1175.
[12] W.D. Kingery, M. Berg, Study of the initial stage of sintering solids by viscous flow, evaporation–condensation, and self diffusion, J. Appl. Phys. 26 (10) (1955) 1205–1212.
[13] R.L. Coble, Initial sintering of alumina, J. Am. Ceram. Soc. 41 (2) (1958) 55–62.
[14] D.L. Johnson, I.B. Cutler, Diffusion sintering: I. Initial stage sintering models and their application to shrinkage of powder compacts, J. Am. Ceram. Soc. 46 (11) (1963) 541–550.
[15] D.L. Johnson, New method of obtaining volume, grain-boundary, and surface diffusion coefficients from sintering data, J. Appl. Phys. 40 (1) (1969) 192–200.
[16] W.H. Rhodes, R.E. Carter, Cationic self-diffusion in calcia-stabilized zirconia, J. Am. Ceram. Soc. 49 (5) (1966) 244–249.
[17] W.S. Young, I.B. Cutler, Initial sintering with constant rates of heating, J. Am. Ceram. Soc. 53 (12) (1970) 659–663.
[18] T.S. Suzuki, Y. Sakka, K. Nakano, K. Hiraga, Effect of ultrasonication on the microstructure and tensile elongation of zirconia-dispersed alumina ceramics prepared by colloidal processing, J. Am. Ceram. Soc. 84 (9) (2001) 2132–2134.
[19] Y. Hirata, I.A. Aksay, Particle segregation during colloidal filtration, in: Proceedings of the Advanced Materials Technology Ceramic Workshop, No. 4, Advances in Materials, Processing, Manufacturing. International Committee for Advanced Materials Technology, Nagoya, Japan, (1988), pp. 3–15.
[20] Y. Sakka, K. Hiraga, Preparation methods and superplastic properties of fine-grained zirconia and alumina based ceramics, Nippon Kagaku Kaishi (8) (1999) 497–508.
[21] K. Matsui, N. Ohmichi, M. Ohgai, T. Yamakawa, M. Uehara, N. Enomoto, J. Hojo, Initial Sintering mechanism of fine zirconia particles including a small amount of alumina, J. Ceram. Soc. Jpn., Supplement 112-1, PacRim5 Special issue 112 (5) (2004) S343–S349.
[22] K. Matsui, K. Tanaka, T. Yamakawa, M. Uehara, N. Enomoto, J. Hojo, Sintering kinetics at isothermal shrinkage: II. Effect of Y_2O_3 concentration on the initial sintering stage of fine zirconia powder, J. Am. Ceram. Soc. 90 (2) (2007) 443–447.
[23] K. Matsui, N. Ohmichi, M. Ohgai, N. Enomoto, J. Hojo, Sintering kinetics at constant rates of heating: effect of Al_2O_3 on the initial sintering stage of fine zirconia powder, J. Am. Ceram. Soc. 88 (12) (2005) 3346–3352.

[24] K. Matsui, A. Matsumoto, M. Uehara, N. Enomoto, J. Hojo, Sintering kinetics at isothermal shrinkage: effect of specific surface area on the initial sintering stage of fine zirconia powder, J. Am. Ceram. Soc. 90 (1) (2007) 44–49.
[25] S.N.B. Hodgson, J. Cawley, M. Clubley, The role of Al_2O_3 impurities on the microstructure and properties of Y-TZP, J. Mater. Process. Technol. 92–93, 85–90 (1999).
[26] E.M. Levin, H.F. McMurdie, in: H.M. Ondik, H.F. McMurdie (Eds.), Al_2O_3–ZrO_2 (cont.); p. 63 (Fig. Zr-084) in Phase Diagrams for Zirconium and Zirconia Systems, American Ceramic Society, OH, 1998.
[27] M.A. Stough, J.R. Hellman, Solid solubility and precipitation in a single-crystal alumina–zirconia system, J. Am. Ceram. Soc. 85 (12) (2002) 2895–2902.
[28] A.J. Burggraaf, A.J. Winnubst, in: J. Nowotny, L.C. Dufour (Eds.), Surface and Near-surface Chemistry of Oxide Materials, Elsevier, Amsterdam, 1988, pp. 449–474.
[29] Y. Ikuhara, T. Yamamoto, A. Kuwabara, H.T. Sakuma, Structure and chemistry of grain boundaries in SiO_2-doped TZP, Sci. Technol. Adv. Mater. 2 (2001) 411–424.
[30] Y. Sakka, Y. Oishi, K. Ando, Zr–Hf interdiffusion in polycrystalline Y_2O_3–$(Zr + Hf)O_2$, J. Mater. Sci. 17 (1982) 3101–3105.
[31] T. Suzuki, Y. Sakka, K. Morita, K. Hiraga, Enhanced superplasticity in alumina-containing zirconia prepared by colloidal processing, Scripta Mater. 43 (8) (2000) 705–710.
[32] Y. Sakka, T. Ishii, T. Suzuki, K. Morita, K. Hiraga, Fabrication of high-strain rate superplastic Yttria-doped zirconia polycrystals by adding manganese and aluminium oxides, J. Eur. Ceram. Soc. 24 (2) (2004) 449–453.
[33] Y. Sakka, T.S. Suzuki, K. Morita, K. Nakano, K. Hiraga, Colloidal processing and superplastic properties of zirconia and alumina based nanocomposites, Scripta Mater. 44 (8) (2001) 2075–2078.
[34] O. Vasylkiv, Y. Sakka, V. Skorokhod, Low-temperature processing and mechanical properties of zirconia and zirconia–alumina nanoceramics, J. Am. Ceram. Soc. 86 (2) (2003) 299–304.
[35] G. Suárez, L.B. Garrido, E.F. Aglietti, Sintering kinetics of 8Y-cubic zirconia: cation diffusion coefficient, Mater. Chem. Phys. 110 (2008) 370–375.